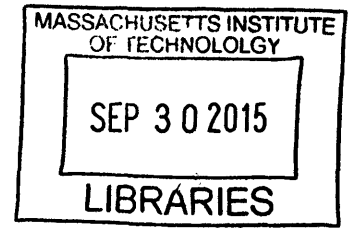


Design for Low Power Irrigation Systems for Small
Plot Farming in Eastern India

ARCHIVES



by

Marcos A. Esparza

Submitted to the Department of Mechanical Engineering
in partial fulfillment of the requirements for the degree of

Bachelor of Science in Mechanical Engineering

at the

MASSACHUSETTS INSTITUTE OF TECHNOLOGY

June 2015

© Massachusetts Institute of Technology 2015. All rights reserved.

¹¹
Signature redacted

Author .

.....
/ ✓ Department of Mechanical Engineering
May 22, 2015

Signature redacted

Certified by

.....
Amos G. Winter V
Assistant Professor
Thesis Supervisor

Signature redacted

Accepted by

Anette Hosoi
Professor of Mechanical Engineering

Design for Low Power Irrigation Systems for Small Plot Farming in Eastern India

by

Marcos A. Esparza

Submitted to the Department of Mechanical Engineering
on May 22, 2015, in partial fulfillment of the
requirements for the degree of
Bachelor of Science in Mechanical Engineering

Abstract

In this thesis, I designed and tested a low-power pump that would be used for drip irrigation on small-scale farms (≈ 1 acre) in Eastern India. The pump is part of a larger irrigation system powered by 300 watts of solar panels and includes batteries as an energy buffer. The pump was designed for and achieved a performance point of 13 gal/min and a pressure head of 1 bar and surpassed the efficiency of every other pump of its kind currently on the market with an efficiency of 29%. The irrigation system is being tested in the field in two pilot studies (ongoing as of this writing since February 2015) in two villages outside of Chakradharpur, Jarkhand, India.

Thesis Supervisor: Amos G. Winter V
Title: Assistant Professor

Acknowledgments

I would first like to thank Kevin Simon and Katherine Taylor, my teammates on this project. We've been working together since the beginning of this low cost irrigation project of which this thesis is just a part of. They've made every portion of this adventure - from traveling around rural India to spending countless ours in lab - very enjoyable and I've learned a lot from them. I'm very excited continue to work with them on the project beyond this thesis.

I would also like to thank Professor Winter for setting us on this course and advising us throughout the project. I would also like to thank Dan Dorsch for his time and the invaluable help he gave us in constructing the pump and the nonprofit, PRADAN, for their help connecting us to farmers for our pilot study. Lastly, I'd like to thank my family for their unending support through this project and my undergraduate career.

Contents

1	Introduction	13
2	Pump Design	19
2.1	Basic Centrifugal Pump Theory	19
2.1.1	Energy Balance	19
2.1.2	Velocity Diagrams and Nondimensional Parameters	21
2.2	Impeller Design	24
2.2.1	Determining Hydraulic Efficiency	24
2.2.2	Outlet Parameters	25
2.2.3	Inlet Parameters	27
2.2.4	Hub and Shroud Geometry	29
2.2.5	Blade Geometry	29
2.2.6	Theoretical Pump Curve	31
2.3	Volute Design	33
3	System Design	39
3.1	Battery Sizing	39
3.2	Motor Selection	42
4	Pump Testing	43
4.1	Experimental Setup	43
4.2	Experimental Results	44
4.3	Pilot Study	46

4.3.1 System Adjustments	46
5 Conclusions and Future Work	49

List of Figures

1-1	Several fallow fields near Chakradharpur in the dry season.	15
1-2	Map of India showing the depth of the water table in each region. . .	16
1-3	Map of India showing the average solar resource in March 2013	17
1-4	A chart showing pumps near the performance point needed to irrigate these small plots.	18
2-1	A CAD model of the designed impeller	20
2-2	A cross-section of the impeller as seen from the top.	22
2-3	A cross-section of the impeller without blades as seen from the side. .	23
2-4	Rotational speed vs. hydraulic efficiency for a flow rate of 16 gpm and head of 1 bar shown by the black solid line. Maximum efficiency of 62.5% at 4390 rpm is shown by the red dotted line.	26
2-5	Chart indicating the type of pump that should be designed based on the specific speed determined by the desired performance point. . . .	27
2-6	Empirical data showing ideal head and exit flow coefficient as a function of specific speed. Ideal head and exit flow coefficient corresponding to this pump is indicated with the red, dotted line.	28
2-7	Width between hub and shroud as a function of radius.	30
2-8	Coordinates for a single impeller blade.	32
2-9	Theoretical pump curve.	33
2-10	CAD model of the volute.	34
2-11	CAD model of a section view of the volute.	35
2-12	A CAD model of the fully assembled pump	36

2-13	The fully assembled pump	37
3-1	Solar power captured by the panels on a typical day and power draw from the pump	40
3-2	Different power flow configurations depending on sunlight throughout the day.	41
3-3	Motor curve showing speed, current, and efficiency as a function of torque.	42
4-1	Diagram of the experimental setup.	43
4-2	Results of pump testing	44
4-3	Results of pump testing	45
4-4	Results of pump testing	45
4-5	Panels, charge controller, motor controller, Arduino Uno, and batteries wired up for use along with some tools for debugging.	47
4-6	Solar panels leaning on a bamboo structure made by the farmers at Sombra.	47
4-7	A plastic lined hole called a jalcund that gets filled with water. The water flowing into the jalcund is being lifted by our pump.	48

Chapter 1

Introduction

Currently, the vast majority of the 23 million small-plot owning farmers (\approx 1-acre) in Eastern India (including the states of Uttar Pradesh, Bihar, West Bengal, Jharkand, and Orissa) are only capable of cultivating their land during one out three of the farming seasons during the year and that is the monsoon season as water is free during that time. During the other two seasons, the winter and "dry" season, they let their lands lay fallow as can be seen in Fig. 1-1. The few that irrigate during the winter season do so with costly and environmentally unfriendly diesel pumps that incur the recurring cost of fuel on the farmers. This cost is so prohibitively expensive that even if farmers choose to irrigate during the winter season, they will forgo irrigating in the "dry" season due to increased water needs.

There is an opportunity to make small solar powered irrigation systems for these farmers. This is due to the fairly constant low water table seen in Fig. 1-2[3] and the vast solar resource that is available to the region, as seen in Fig. 1-3[1]. Pumps powered by solar power exist but are over-sized for the amount of water needed by these 23 million small plot farmers. They are often systems larger than 1 kilowatt which leads to a large number of solar panels that a small farmer cannot afford. The goal of this project is to design and test an irrigation system specifically fit for a 1 acre farm. This design requirement fixes the water needed at about 5,300 gallon per day assuming that the farmers are in the driest part of Eastern India and irrigating the most water intensive crops.[4] If the farmer were to irrigate for seven hours out of the

day, this would amount to a flow rate of 13 gal/min.

Now that the flow rate of the irrigation system has been determined, the needed pressure head can be found. Eastern India was chosen specifically because it should have much higher agricultural productivity than it currently does because of its fairly constant shallow water table and solar resource previously mentioned. Predominantly, the water level is no more than ten meters deep so the system should be designed to provide 1 bar of pressure head as that corresponds to about 10 meters of lift. With these two design points determined the power draw of the pump can be found to be 235 watts if the pump is assumed to be 35% efficient, which will be shown to be a realistic efficiency in Chapter 2.

This pump can be powered by 300 watts of solar panels and a pair of sealed lead acid motorcycle batteries that act as an energy buffer. The design of the pump is described in Chapter 2, the rest of the system design is detailed in Chapter 3, experiments and pump testing is reported in Chapter 4, and conclusions and future work are in Chapter 5.



Figure 1-1: Several fallow fields near Chakradharpur in the dry season.

Depth to Water Level Map (Pre Monsoon - 2014)

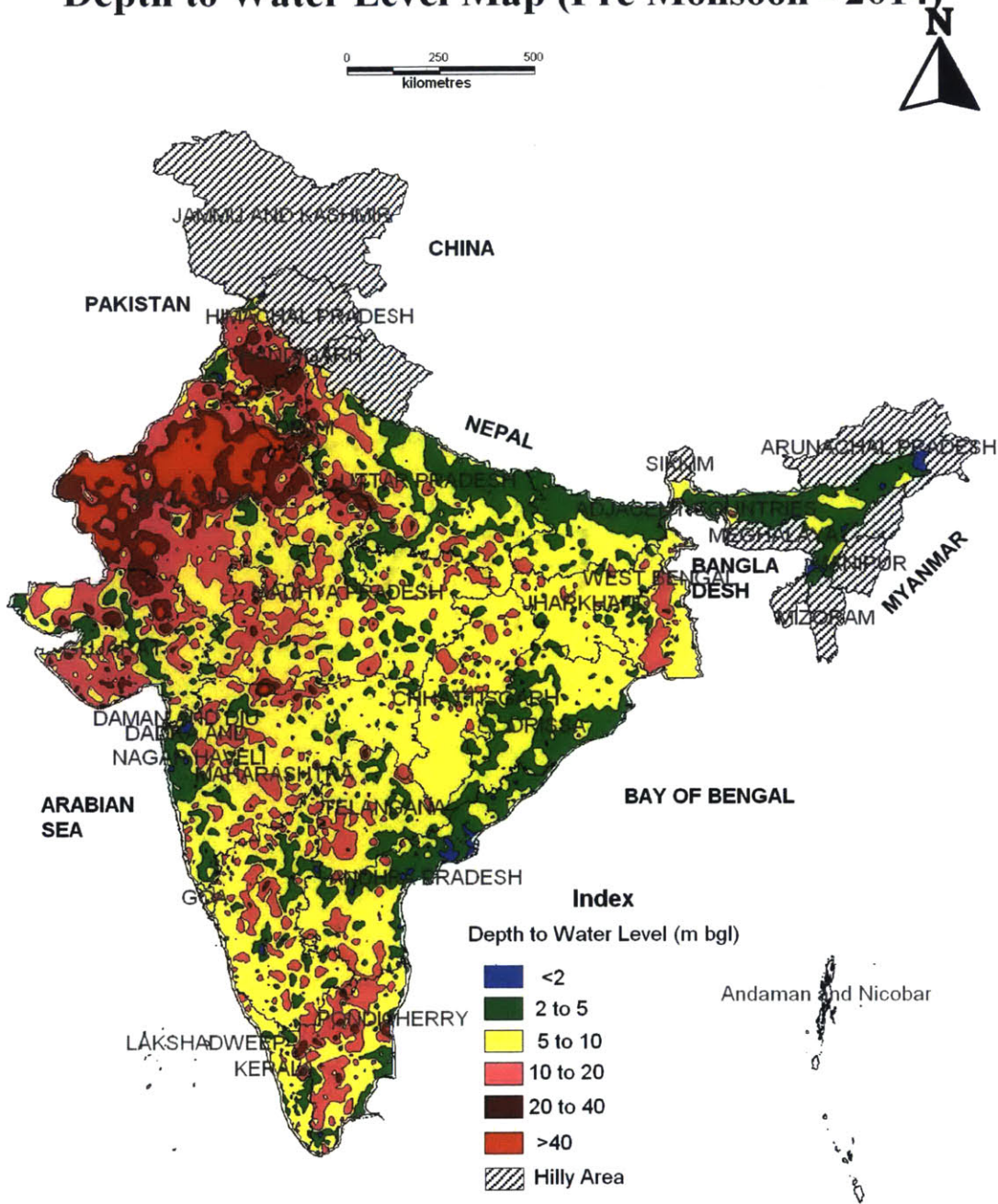


Figure 1-2: Map of India showing the depth of the water table in each region.

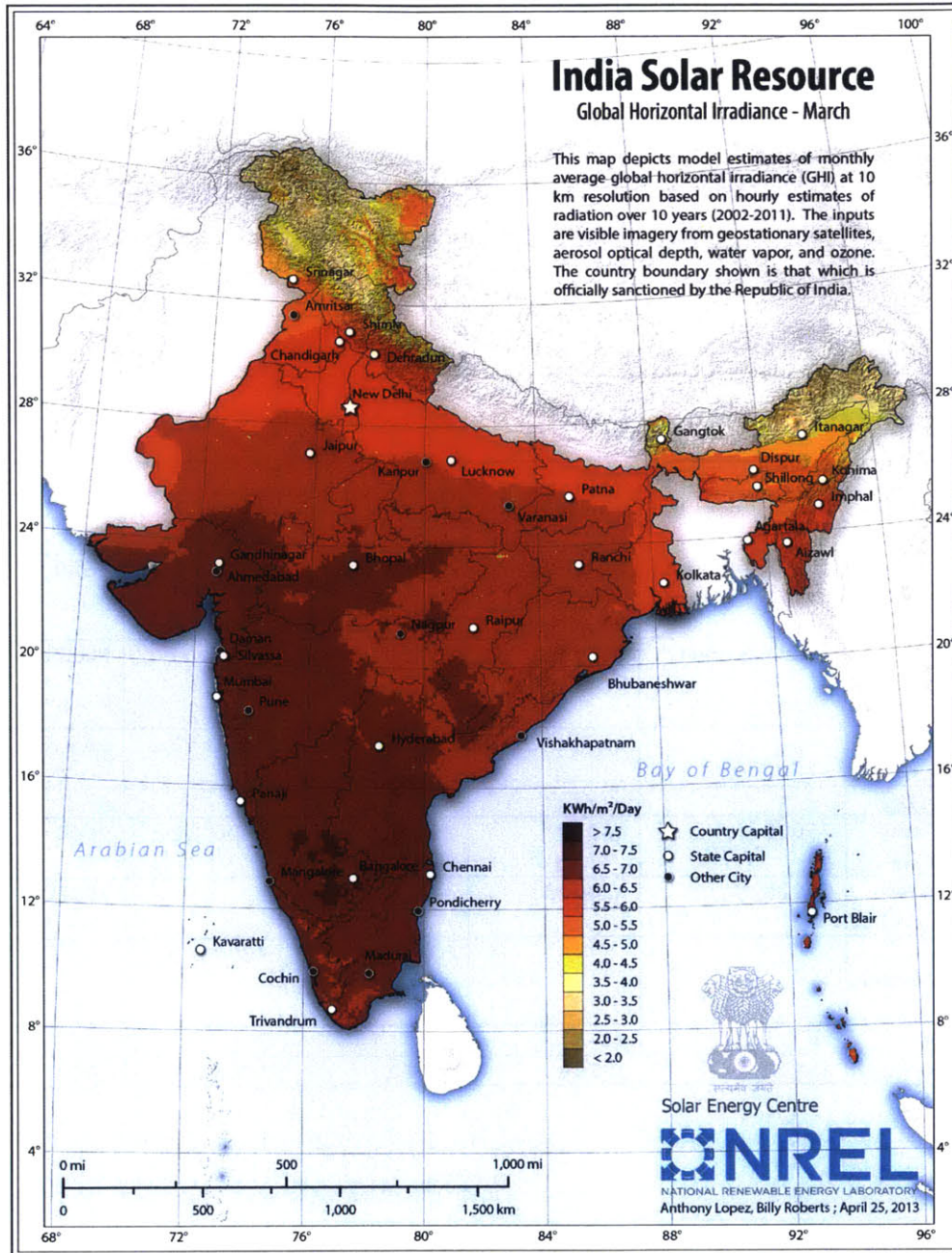


Figure 1-3: Map of India showing the average solar resource in March 2013

Company and Model	Rotomag RS1200 Submersible ^[1]	Rotomag MBP60 Surface ^[1]	Honda WX10K1A ^[2B]	Taizhou, Nimbus 50KB ^[4B]	Ours
Type	Solar, Centrifugal, DC	Solar, Centrifugal, DC	Diesel, Centrifugal	Diesel	Solar, Centrifugal, DC
HP	1	2	1 ^[3B]	3.4	1/3
Motor Capacity (W)	800	1500			185 ^[4B]
Panel/Plate Requirement (W)	1200	1800			300
PV voltage	110V	60V			24V
Max Total Head (m)	30	15	35	26	18
Max Discharge (L/hr)	12,000 (at 20m head)*	24,000 (at 10m head, 7.5hr day)*	8400	22,000	4680
Material	Stainless steel	Stainless Steel	Aluminum and Ceramic	Metal	Plastic
Size (cm)			33 x 23 x 30	53.5 x 42 x 51	25 x 11 x 11
Weight (kg)			6	27	4
Price (Pump Only) in Rs	75000	43000	29000	5400** ^[5B]	9000
Price Panels (63 INR/W)	76000	114000			19000
Price Diesel/Yr/Acre			32000	48000	
Lifetime	10	10	7	3	10
Price/yr Total	15100	15700	36000	50000	2800

Figure 1-4: A chart showing pumps near the performance point needed to irrigate these small plots.

Chapter 2

Pump Design

The proposed solar-powered pump system has an operating point of 13 gal/min at a pressure of 1 bar. In order for the system to be economical, the pump must be 35% efficient, requiring only 235 watts of power. The process of designing this pump was followed as outlined in *Pump Handbook* [5], an invaluable resource for engineers looking to design pumps. Before diving into the design of the pump I will discuss basic centrifugal pump theory (Section 2.1). I will then continue with the impeller design (Section 2.2), followed by volute design (Section 2.3). Motor selection will be discussed in the following chapter.

2.1 Basic Centrifugal Pump Theory

2.1.1 Energy Balance

The internal flow of a centrifugal pump is often turbulent, has three-dimensional components, and is locally unsteady. However it is possible to use one-dimensional analysis to approximate the performance of a particular pump. We begin by looking at an energy balance, Eq. (2.1), in a control volume consisting of the volute of the pump¹.

¹Heat transfer in and out of the control volume is neglected as the system is assumed to be adiabatic

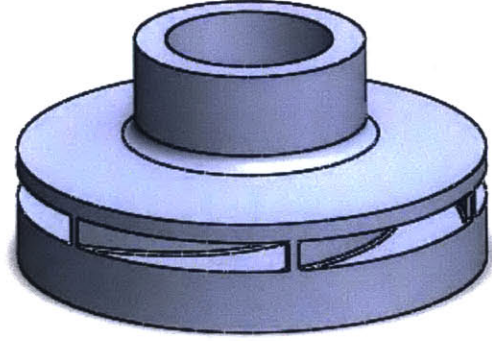


Figure 2-1: A CAD model of the designed impeller

$$\frac{P_E}{\dot{m}} = g\Delta H + \Delta u \quad (2.1)$$

In Eq. (2.1), P_E represents the electrical power going into the pump and ΔH represents the change in total dynamic head, Eq. (2.2), from the inlet to the outlet of the pump. Δu is the change in thermal energy and is not a useful kind of energy transfer for this system and represents the inefficiencies of the pump, and g is the acceleration due to gravity. This total dynamic head includes the static pressure head, velocity head, and the elevation head.

$$H = \underbrace{\frac{p}{\rho g}}_{\text{static pressure head}} + \underbrace{\frac{V^2}{2g}}_{\text{velocity head}} + \underbrace{Z}_{\text{elevation head}} \quad (2.2)$$

In Eq. (2.2), p is the static pressure at the outlet of the volute, V is the velocity of the water at the volute outlet, and Z is the elevation difference between the inlet of the pump and the point of the irrigation system in which the water reaches atmospheric pressure. As can be seen in Eq (2.1), not all of the power goes into the change in total dynamic head. The efficiency of the pump is then represented by Eq. (2.3). As the goal of this project is to design a very efficient pump, it is important to look at all sources of inefficiencies. Eq (2.4) shows all the sources of inefficiencies in the pump including the motor efficiency η_e , the mechanical efficiency η_m , the hydraulic

efficiency η_h , and the volumetric efficiency η_v .

$$\eta = \frac{g\Delta H\dot{m}}{P_E} \quad (2.3)$$

$$\eta = \underbrace{\frac{P_S}{P_E}}_{\text{motor efficiency, } \eta_e} \times \underbrace{\frac{P_I}{P_S}}_{\text{mechanical efficiency, } \eta_m} \times \underbrace{\frac{\Delta H}{\Delta H_i}}_{\text{hydraulic efficiency, } \eta_h} \times \underbrace{\frac{Q}{Q + Q_L}}_{\text{volumetric efficiency, } \eta_v} \quad (2.4)$$

In Eq. (2.4), ΔH_i is the ideal pump head, Q is the flow rate, and Q_L is the lost flow due to leakage. At each step of the pump design process, attempts were made to mitigate each of these inefficiencies. At this initial pump design stage of determining the impeller geometry, maximizing hydraulic efficiency was the goal.

2.1.2 Velocity Diagrams and Nondimensional Parameters

Before going further, it is important to complete our vocabulary regarding pump design. Fig. 2-2 depicts a bird's eye view of the blades of the impeller with a velocity diagram of the water at the tip of one of the blades. The resultant vector V is made up by the addition of two velocities: U_2 the velocity of the water tangent to the circumference of the impeller and W_2 the velocity of the water tangent to the blade. V can also be broken up into its normal components: the meridional flow $V_{m,2}$ and its tangential flow $V_{\theta,2}$. Fig. 2-3 shows a cross-section of the impeller the general dimensions of the pump: the outer radius r_2 , the radius of the inlet (also known as eye) r_e , and the width at the exit b_2 .

In order to greatly simplify the process of pump design, dimensionless variables are used and can be seen in Eq. (2.5)-(2.9).

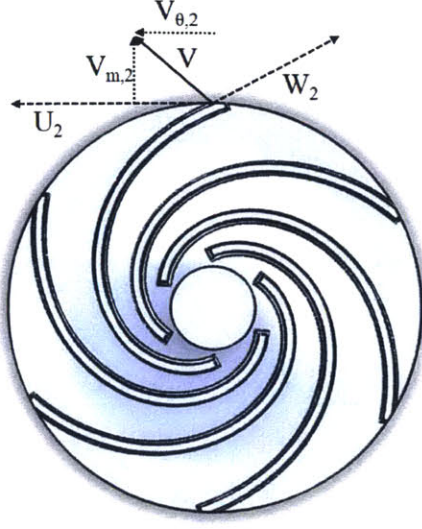


Figure 2-2: A cross-section of the impeller as seen from the top.

$$Q_s = \frac{Q}{\Omega r_2^3} \quad \text{Specific Flow} \quad (2.5)$$

$$\psi = \frac{g\Delta H}{\Omega^2 r_2^2} \quad \text{Head Coefficient} \quad (2.6)$$

$$\phi_2 = \frac{V_{m,2}}{U_2} = \frac{Q}{2\pi\Omega r_2^2 b_2^2} \quad \text{Exit Flow Coefficient} \quad (2.7)$$

$$\phi_e = \frac{\bar{V}_e}{U_e} = \frac{Q/A_e}{\Omega r_e} = \frac{Q}{\pi\Omega r_e^3} \quad \text{Inlet Flow Coefficient} \quad (2.8)$$

$$\tau = \frac{2gNPSH}{\Omega^2 r_2^2} \quad \text{Cavitation Coefficient} \quad (2.9)$$

In Eq. (2.5)-(2.9) Ω is the angular velocity of the impeller, g is the gravitational constant, \bar{V}_e is the average meridional flow at the inlet, U_e is the tangential velocity at the inlet, A_e is the area of the inlet opening², and NPSH is the net positive suction

²In this case $A_e = \pi r_e^2$ as the hub (as seen in 2-3) comes to a point at the center. If this wasn't the case then $A_e = \pi(r_e^2 - r_s^2)$ where r_s is the radius of the shroud at the inlet. In our case, $r_s = 0$

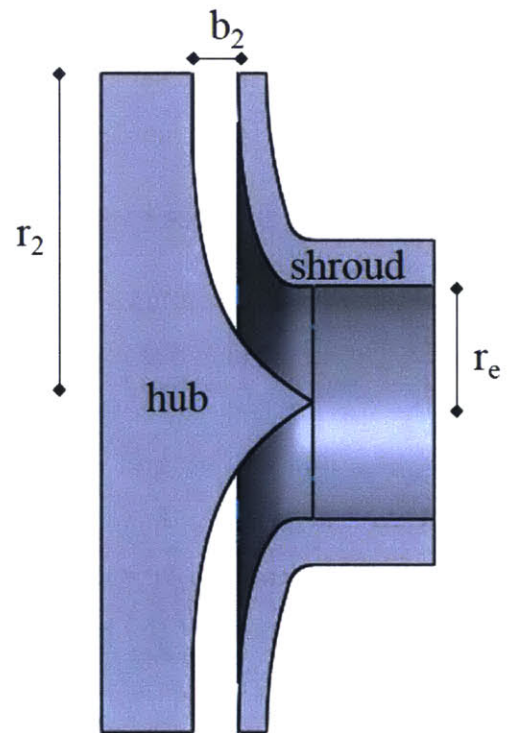


Figure 2-3: A cross-section of the impeller without blades as seen from the side.

head, given by Eq. (2.10)

$$\text{NPSH} = \frac{P_{in} - p_v}{\rho g} \quad (2.10)$$

$$= 9.87 \text{ meters} \quad (2.11)$$

where P_{in} is the atmospheric pressure (1 bar) and p_v is the vapor pressure of water (0.032).

2.2 Impeller Design

2.2.1 Determining Hydraulic Efficiency

When designing the impeller, I attempted to optimize the hydraulic efficiency, η_h , about the performance point, $Q = 16 \text{ gpm}^3$ and $\Delta H = 1 \text{ bar}$. The optimal shape of the impeller is determined by the specific flow, Q_s of the pump when there is negligible viscous influence, no two-phase fluid effects, and no solid particles in the flow. However, the designer will not know the radius of the impeller or the angular velocity at this stage of the design process. For this reason, the square root of the specific flow (Eq. (2.5)) can be divided by the $\frac{3}{4}$ -power of the head coefficient (Eq. (2.6)), ψ in order to cancel out the radius term r_2 in each parameter. The resulting parameter the specific speed and is given by Eq. (2.12).

$$N_s = \frac{N(\text{rpm}) * \sqrt{Q(\text{gpm})}}{\Delta H(\text{ft})^{3/4}} = \frac{\sqrt{Q_s}}{\psi^{3/4}} \quad (2.12)$$

Although we have eliminated the radius term in our parameter, the speed at which the impeller will spin is also unknown at this point. Fortunately, an empirical correlation that relates efficiency to impeller speed exists [2] and is given by Eq. (2.13).

³A flow rate of 16 gpm was used instead of 13 gpm as it was found that the design process was not perfect and the design point of the flow rate needed to be overestimated in order to achieve the desired flow rate

$$\eta_h = 0.94 - 0.08955 \times \left[\frac{Q(\text{gpm})}{N(\text{rpm})} \times X \right]^{-0.21333} - 0.29 \times \left[\log_{10} \left(\frac{2286}{N_s} \right) \right]^2 \quad (2.13)$$

The impeller speed, N , was plotted versus the hydraulic efficiency η_h of the impeller for our desired flow rate and can be seen in Fig. 2-4. The optimal impeller speed and specific speed were calculated to be 4390 rpm and 1281 respectively and gave a maximum hydraulic efficiency of 62.5%. The specific speed also indicates the type of pump that should be designed as can be seen in Fig 2-5. Our specific speed of 1281 indicates that a centrifugal pump is the pump that should be built.⁴ Due to the motor selection that will be described in Chapter 3, the actual impeller speed was 4000 rpm leading to a specific speed of 1170. As can be seen in Fig. 2-4, this variation in speed leads to a negligible decrease in maximum hydraulic efficiency.

2.2.2 Outlet Parameters

Now that the speed and type of pump to be designed has been determined, the impeller can now be sized. By rearranging Eq.(2.6) and (2.7) it can be seen that the outlet parameters r_2 and b_2 can be determined once the pump head coefficient, ψ , and the impeller exit, ϕ flow are found.

$$r_2 = \frac{1}{\Omega} \sqrt{\frac{g\Delta H}{\psi}} \quad (2.14)$$

$$b_2 = \frac{Q}{2\pi\Omega r_2^2 \phi} \quad (2.15)$$

This can be done using existing empirical correlations between the pump head and flow coefficients and the metric specific speed. (Eq. (2.6)-(2.7))and the metric specific speeds (in this case $\Omega a_s = 0.41$) of the impeller. [7].

⁴One may also notice that a screw pump could also be used for our application and it could be argued that its superior efficiency would make it a better choice. However, its construction requires precision parts which greatly increases the cost of the pump. For this reason it was not chosen.

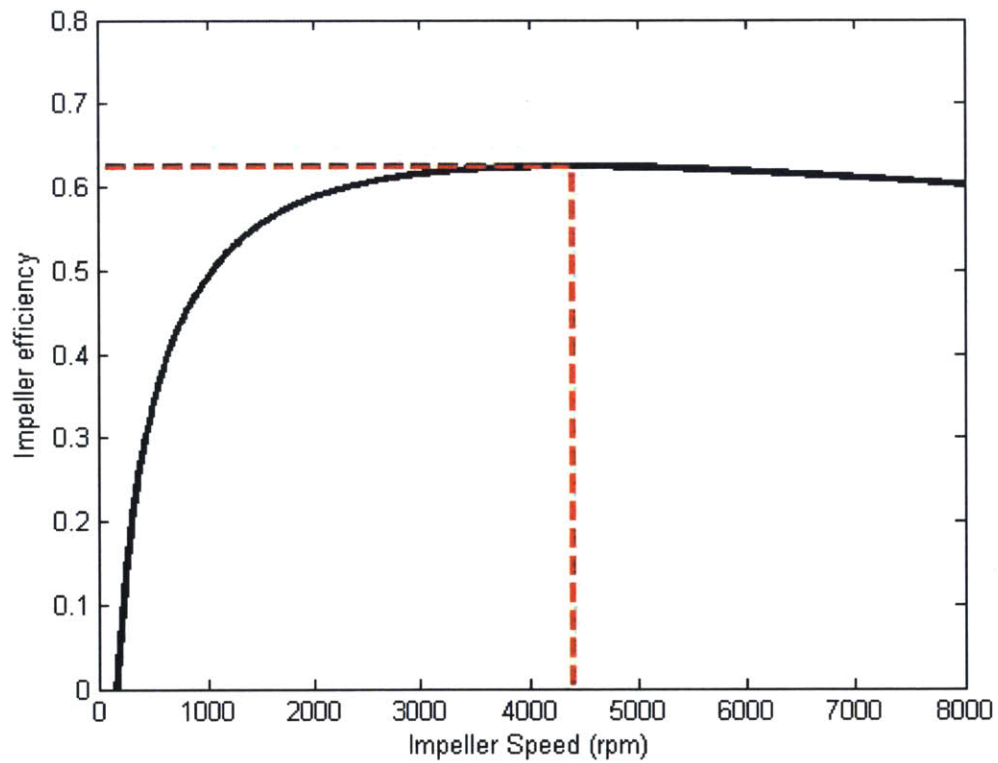


Figure 2-4: Rotational speed vs. hydraulic efficiency for a flow rate of 16 gpm and head of 1 bar shown by the black solid line. Maximum efficiency of 62.5% at 4390 rpm is shown by the red dotted line.

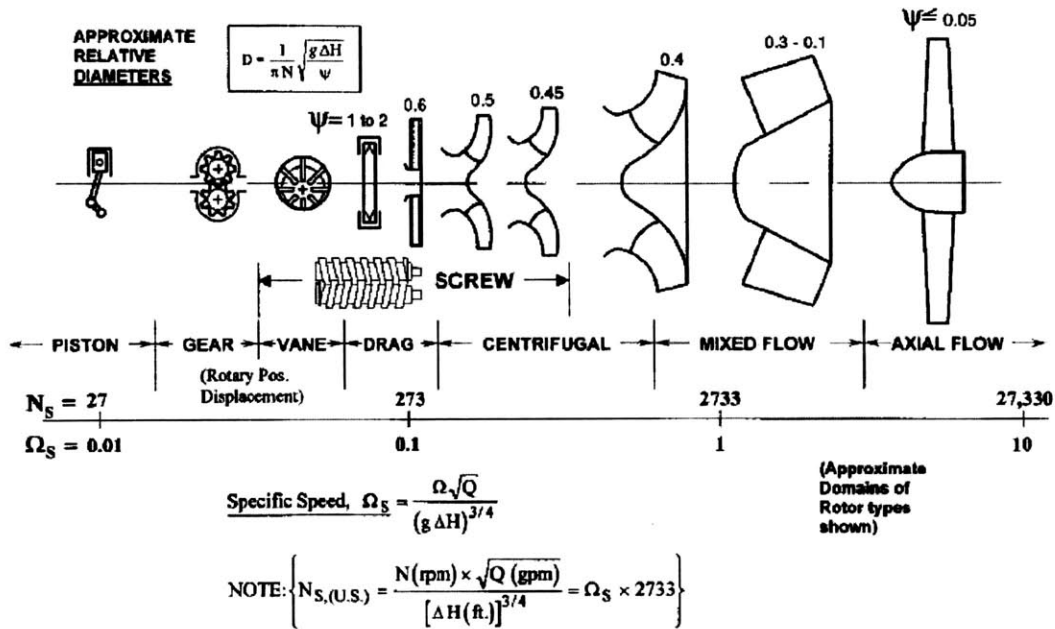


Figure 2-5: Chart indicating the type of pump that should be designed based on the specific speed determined by the desired performance point.

The correlation of the ideal head and flow coefficients vs. the metric specific speed can be seen in Fig.2-6. Using these correlations, the head coefficient and the outer radius were calculated to be $\psi = 0.49$ and $r_2 = 1.51$ inches respectively. The channel height at the exit can also be calculated from the ideal impeller exit flow coefficient which is calculated to be $\phi = 0.11$, indicating a channel height of $b_2 = 0.20$ inches at the outer edge of the impeller.

2.2.3 Inlet Parameters

Next, in order to determine the inlet radius r_e , we must use the cavitation (Eq. (2.9)) and inlet flow (Eq. (2.8)) coefficient. Empirical data exists for the ideal cavitation coefficient as a function of the inlet flow coefficient and is shown in Eq. (2.16)[5]. The specific suction speed Ω_{ss} (similar but not the same to specific speed) must also be used. Ω_{ss} can already be calculated directly using known values (Eq. (2.17)) but

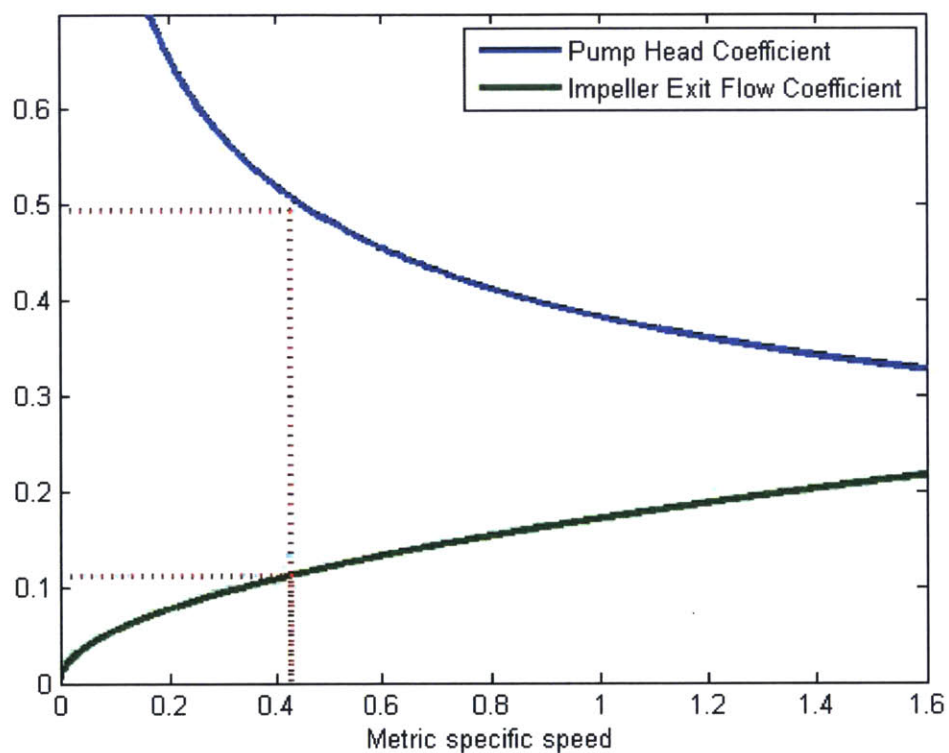


Figure 2-6: Empirical data showing ideal head and exit flow coefficient as a function of specific speed. Ideal head and exit flow coefficient corresponding to this pump is indicated with the red, dotted line.

Eq. (2.8) and (2.9) can also be rearranged in order to give Ω_{ss} in terms of ϕ_e and τ .

$$\tau = 1.792\phi_e^2 + 0.102 \quad (2.16)$$

$$\Omega_{ss} = \frac{\Omega\sqrt{Q}}{(gNPSH)^{3/4}} \quad (2.17)$$

$$= \frac{\sqrt{\pi\phi_e}}{(\tau/2)^{3/4}} \quad (2.18)$$

$$r_e = \left(\frac{Q}{\pi\Omega\phi_e}\right)^{1/3} \quad (2.19)$$

Using the empirical correlation (Eq. (2.16)) and an iterative solver, a solution for ϕ_e was found so that Eq. (2.17) and (2.18) are equivalent. ϕ_e was found to be 0.31 and r_e was found to be 0.503 inches.

2.2.4 Hub and Shroud Geometry

Now that the general dimensions of the impeller have been determined, we can now find the shape of the hub and shroud. The restrictions on the design of the shroud are pretty loose and only require that the minimum curvature of the shroud is less than the inlet radius $r_e = 0.503$ inches. The width between the shroud and the hub should be designed so that the meridional velocity (and therefore the cross-sectional area) increases linearly.[5] The height of the channel as a function of radius can be seen in Fig 2-7.

2.2.5 Blade Geometry

Finally, the blade geometry must be determined. There are a few different techniques to determine blade geometry including those in which blade angle changes with height at the same radius so that the blade is tilted. However, for this application a simplified technique was used in which the blade geometry is constant with height. This was to facilitate future ease in manufacturing as the current 'simplified' impeller can more easily be made in two parts using injection molding. This would be much more

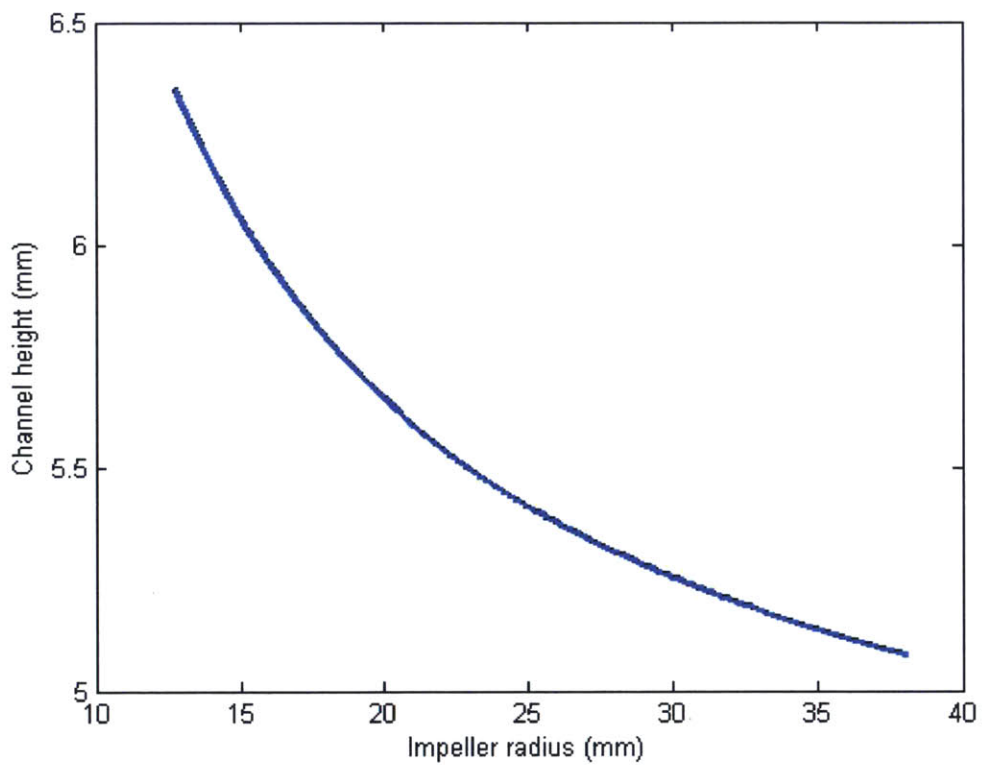


Figure 2-7: Width between hub and shroud as a function of radius.

difficult if the blades were tilted.

A constant blade angle of $\beta = 22.5^\circ$ was chosen according to [5]. The polar coordinates of the blades can be determined using a summation of a discrete form of Eq. (2.20).

$$d\theta = \frac{dr}{r \tan(\beta)} \quad (2.20)$$

Figure 2-8 shows the coordinates of a single blade on the impeller. The number of blades can be determined using Eq. (2.21). The number of blades is important as it influences the pressure difference between blades; too great a pressure difference can lead to cavitation.

$$\sigma = \frac{n_b \times l}{2\pi r_2} \quad (2.21)$$

In Eq. (2.21), σ is the solidity, and l is the arc length of the blade (which for our case is $l = 2.69$ inches). For a pump of our specific speed, its recommended that the solidity is about 1.8.[5] With six blades ($n_b = 6$) the solidity is $\sigma = 1.94$. This is closer to 1.8 than when using any other integer value for n_b . The designed impeller can be seen in both Fig. 2-1,2-2, and 2-3.

2.2.6 Theoretical Pump Curve

A conservative theoretical pump curve can be constructed using the ideal head equation (2.22) and multiplying the result by the empirical hydraulic efficiency (2.23) at every flow rate.[5] The theoretical pump curve for our pump can be seen in Fig 2-9. This curve assumes perfect efficiency at all other points of the pump (motor, leakage etc.) so it is expected that the maximum head reached is higher than our target of 1 bar. Also, the pressure head will not go to zero as flow rate goes to zero as ,in reality, the lack efficiency will instead translate into loss of flow rate rather than pump head at this low flow rate. Instead it will likely be larger than the max shown, the empirical formula (2.23) does not capture this. This not our operating point so this discrepancy is unimportant.

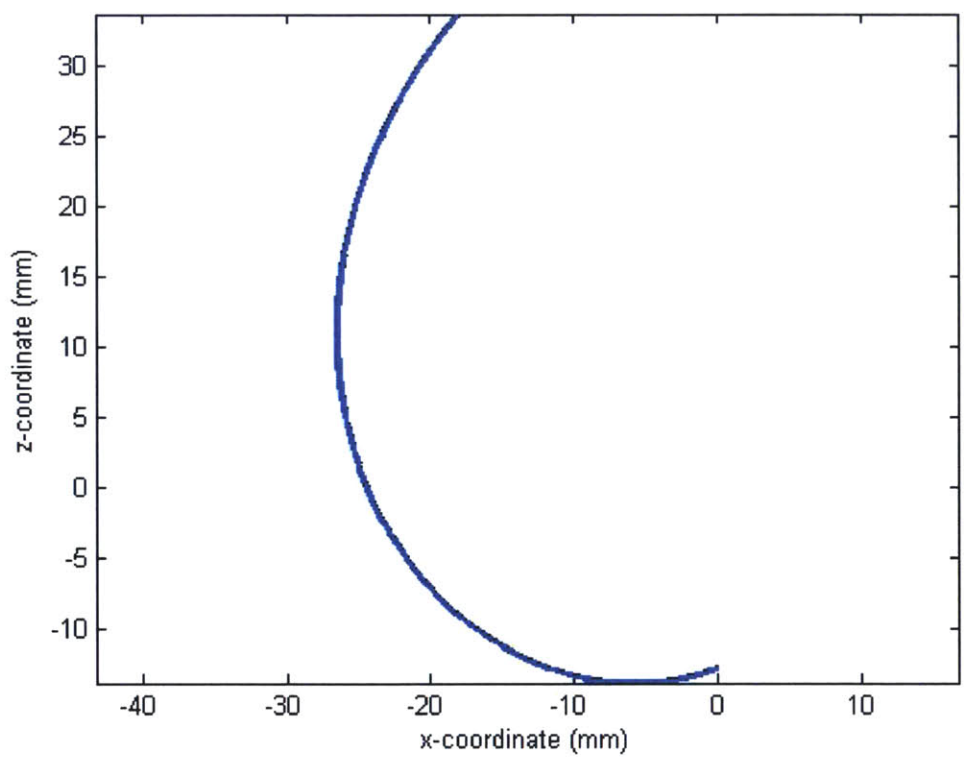


Figure 2-8: Coordinates for a single impeller blade.

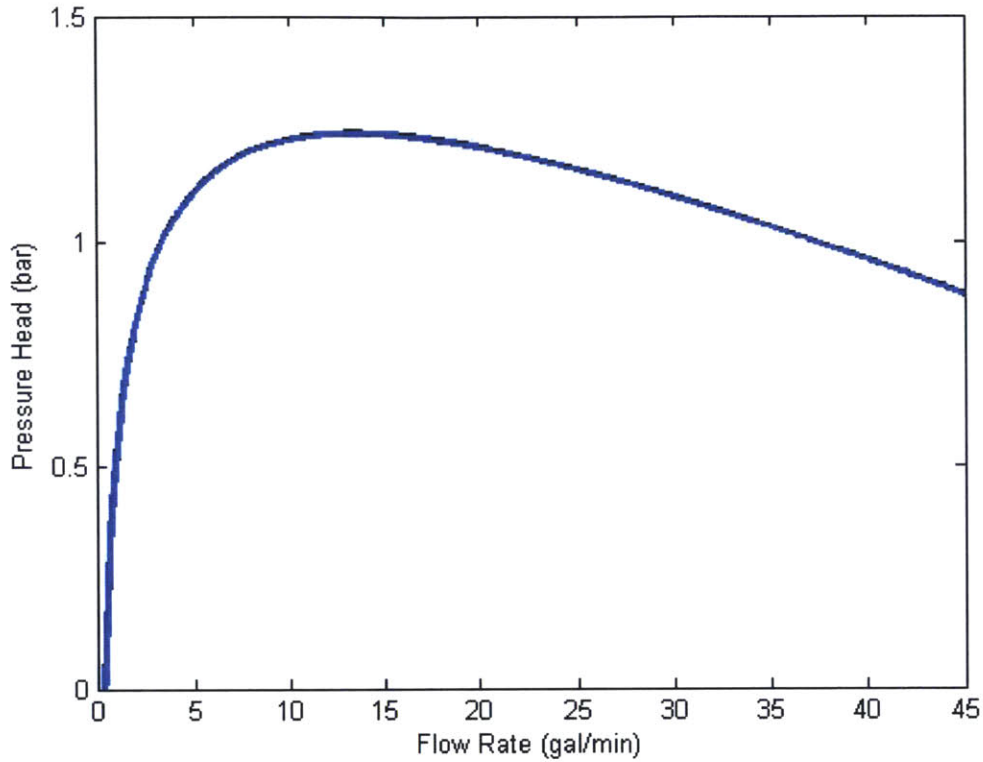


Figure 2-9: Theoretical pump curve.

$$H = \frac{U_2^2}{g} - \frac{U_2 \cot(\beta)Q}{1\pi r_2 b_2 g} \quad (2.22)$$

$$\eta_{hy} = 1 - 0.8/Q[\text{gpm}]^{0.25} \quad (2.23)$$

2.3 Volute Design

The volute (Figure 2-10) converts the rotational kinetic energy of the water into a desired pressure head. Kevin Simon took the lead on the volute design but I will include a brief description of the process for completeness. A more detailed explanation of the process can be found in his thesis.[6] In order to mitigate recirculation and progressive acceleration the pressure head must remain constant at every point

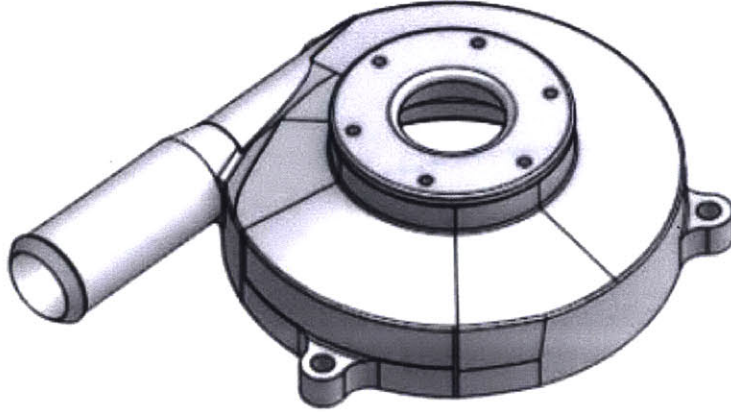


Figure 2-10: CAD model of the volute.

θ along the edge of the impeller. In order to do this, the cross section of the path the water takes in the volute must increase proportionately as it makes its way around the volute as shown in Eq. (2.24). Fig.2-11 shows this linear increase of cross section along the circumference of the impeller.

$$A_{vol}(\theta) = \frac{Q(\theta)}{V_{\theta}(\theta)} \quad (2.24)$$

$$Q(\theta) = Q(2\pi) \frac{\theta}{2\pi} \quad (2.25)$$

$$V_{\theta}(\theta) = \frac{V_{\theta}(2\pi)r(2\pi)}{r(\theta)} \quad (2.26)$$

Fig. 2-12 shows a model of the fully assembled pump. The volute was made out a ABS plastic with a FDM 3D printer. In order to prevent leakage through the plastic and increase the volumetric efficiency, a combination coating the volute in epoxy and an acetone vapor bath was used. Fig. 2-13 shows the fully assembled pump and the resulting smooth features on the volute is a result from the painting and acetone vapor bath.

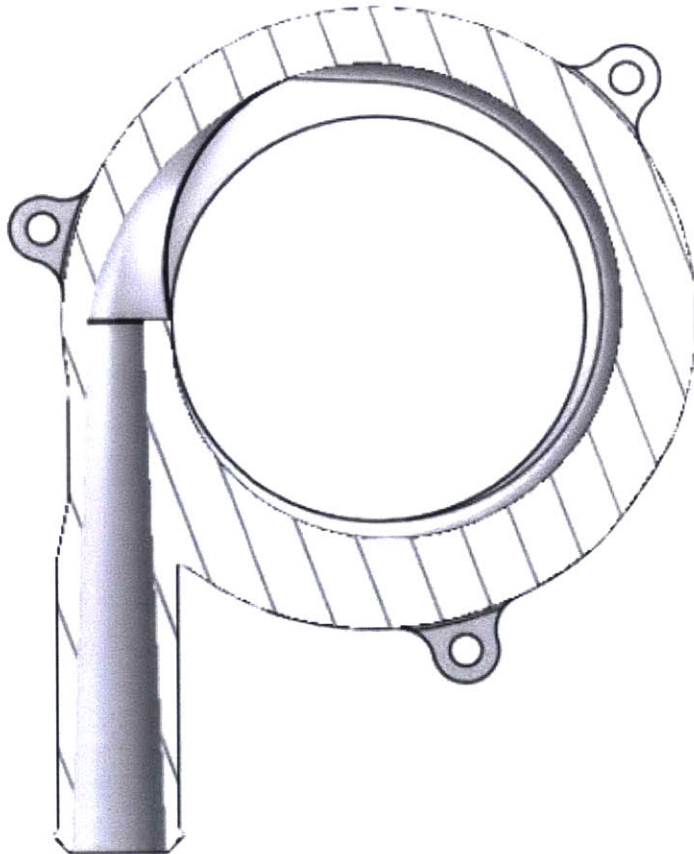


Figure 2-11: CAD model of a section view of the volute.

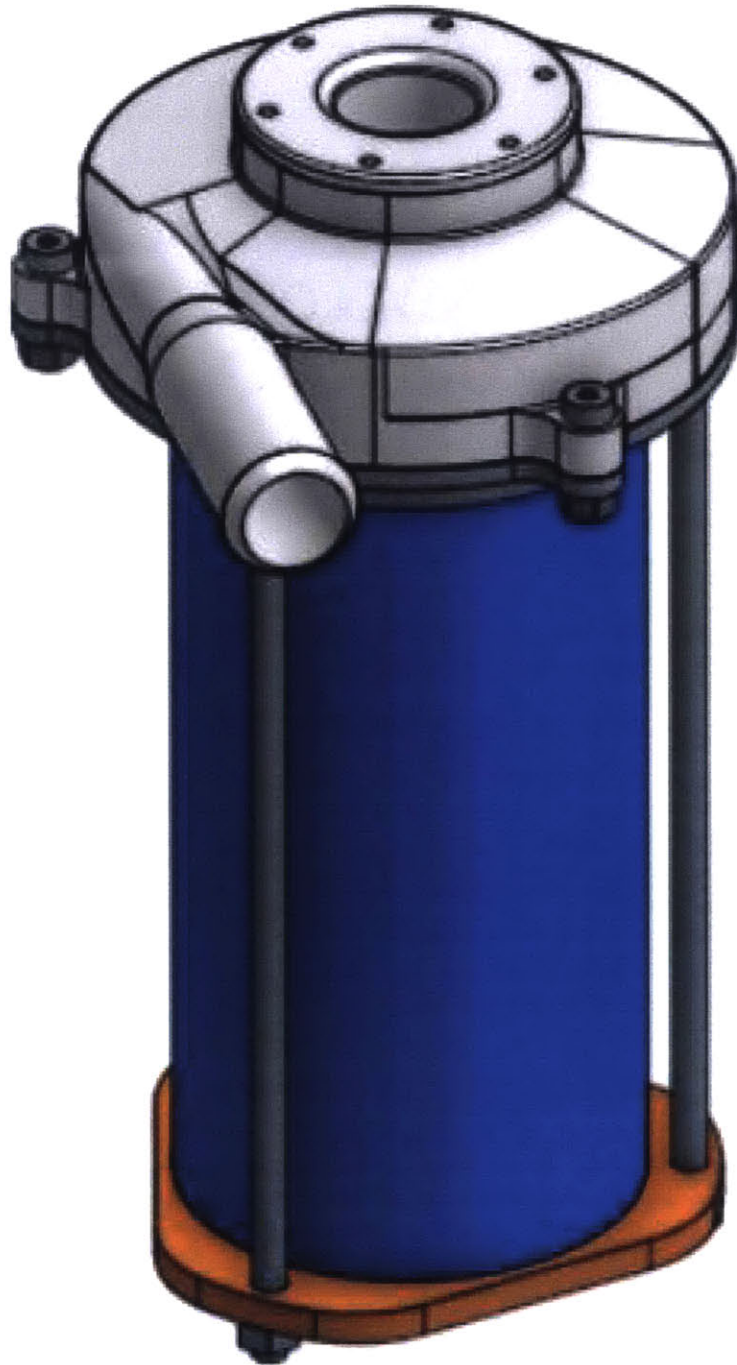


Figure 2-12: A CAD model of the fully assembled pump

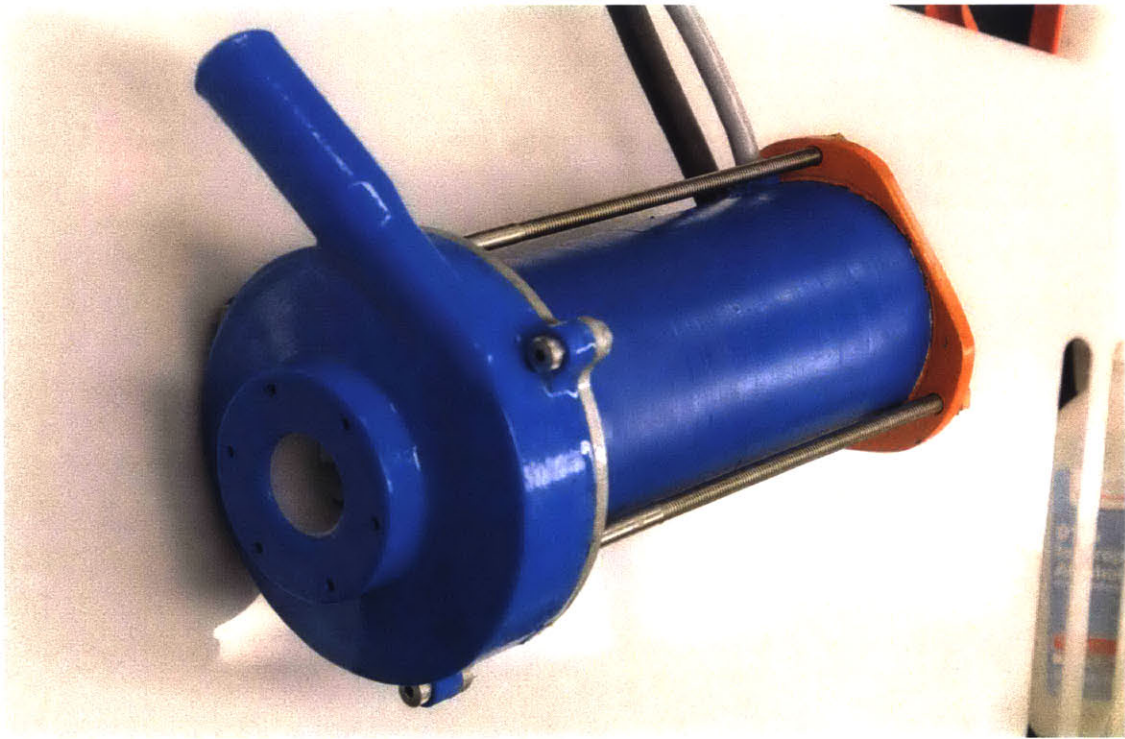


Figure 2-13: The fully assembled pump

Chapter 3

System Design

3.1 Battery Sizing

The irrigation system consists of the pump described in the previous chapter, 300 watts of solar panels, a charge and motor controller, and batteries that act as an energy buffer. The batteries are necessary because, as seen in Fig. 3-1, the captured solar power is not constant and is more often than not greater or less than the power necessary to run the pump. The battery assists the pump during the times when it is running but there is not enough sunlight to run the pump solely off the panels (Fig. 3-2c). When there is more sunlight than is necessary, the extra power is stored in the battery (Fig. 3-2a). Lastly, at the beginning and end of the day, when there is low sun and the pump is off, the power from the panels is again stored in the battery for when it is needed (Fig.3-2b). The size of the battery can be determined by measuring the difference in the curves of Fig. 3-1 at one point where the power draw is greater than the solar radiation. Assuming that we only discharge the batteries by 30% in order to allow them to last longer, 131.6 watt-hours are needed to ensure that the pump can run when there is not sufficient sunlight. For a 12-volt battery this corresponds to about 11 amp-hours which is a little less than two motor cycle batteries (each being 7 amp-hours).

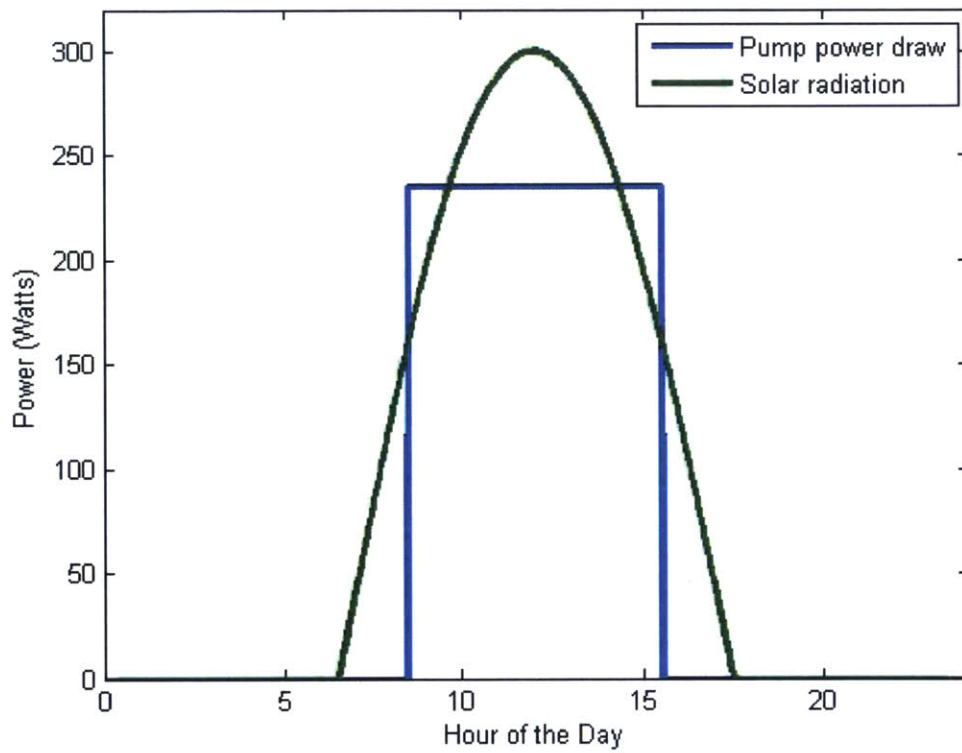
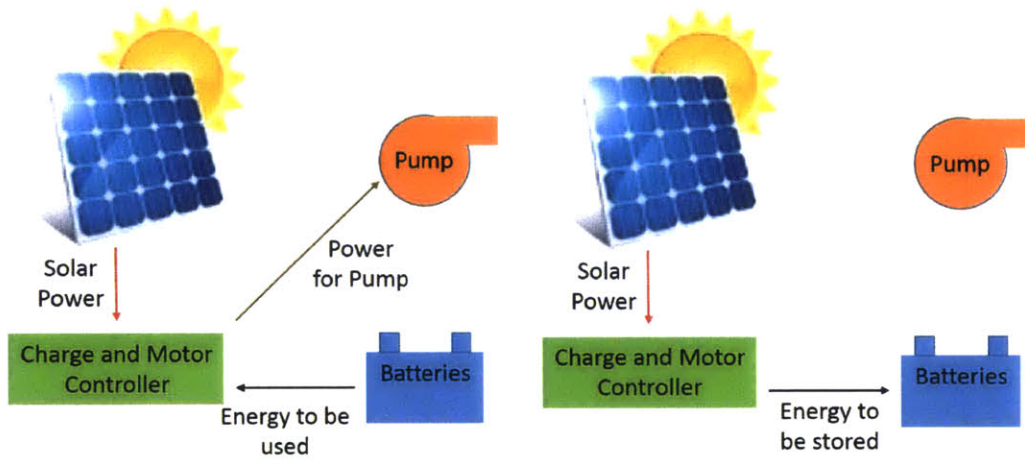
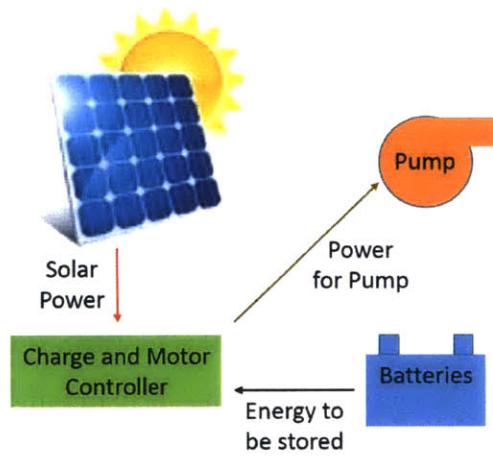


Figure 3-1: Solar power captured by the panels on a typical day and power draw from the pump



(a) Power flow configuration at peak sunlight times. (middle of the day)

(b) Power flow configuration at low sunlight times (beginning and end of the day).



(c) Power flow configuration at times of medium sunlight.

Figure 3-2: Different power flow configurations depending on sunlight throughout the day.

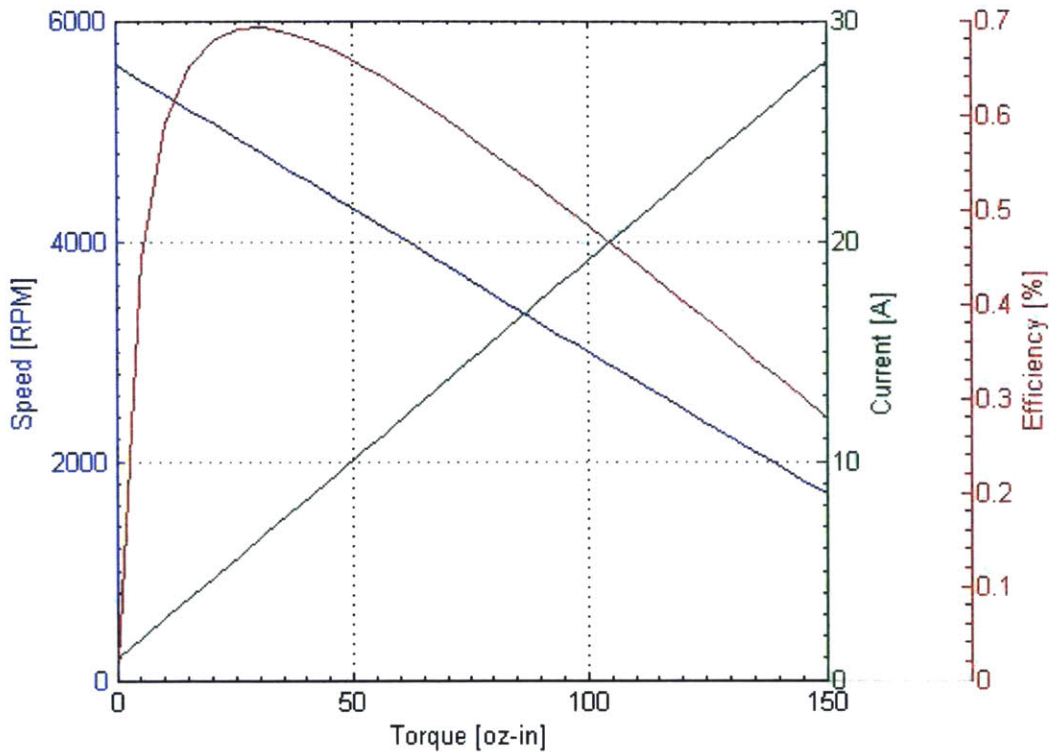


Figure 3-3: Motor curve showing speed, current, and efficiency as a function of torque.

3.2 Motor Selection

A brushless DC motor was chosen from Anaheim Automation.¹ A brushless motor was chosen over a brushed motor because of its longer lifetime and its higher efficiency. It was selected as it had a rated speed of 4000 rpm which is close to are design point of 4390 rpm and it had the necessary torque to maintain that speed. Using the manufacturer supplied motor specifications, a motor curve could be created and is seen in Fig. 3-3. As can be seen on the curve, at our performance point of 4000 rpm, the efficiency is 62%. The effect of this low efficiency will be discussed further in Section 4.2.

¹Model # BLWS65235S-24V-400

Chapter 4

Pump Testing

4.1 Experimental Setup

The pump was tested using a basic fluid circuit shown in Fig. 4-1. It included the pump in a basin full of water, a pressure gauge¹, a valve to control the line pressure and a flow meter². The voltage supplied to the pump was controlled by a DC power supply and current was measured with a clamp-on ammeter³.

¹High-Accuracy Pressure Gauge supplied by McMaster (product #4007K2) with an accuracy of $\pm 0.5\%$.

²Omega FTB792 with an accuracy of $\pm 1.5\%$.

³Fluke 373 True-RMS Clamp-On meter with an error of $\pm 1\%$.

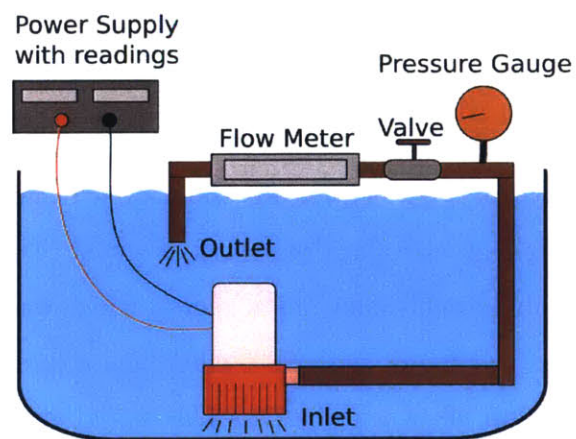


Figure 4-1: Diagram of the experimental setup.

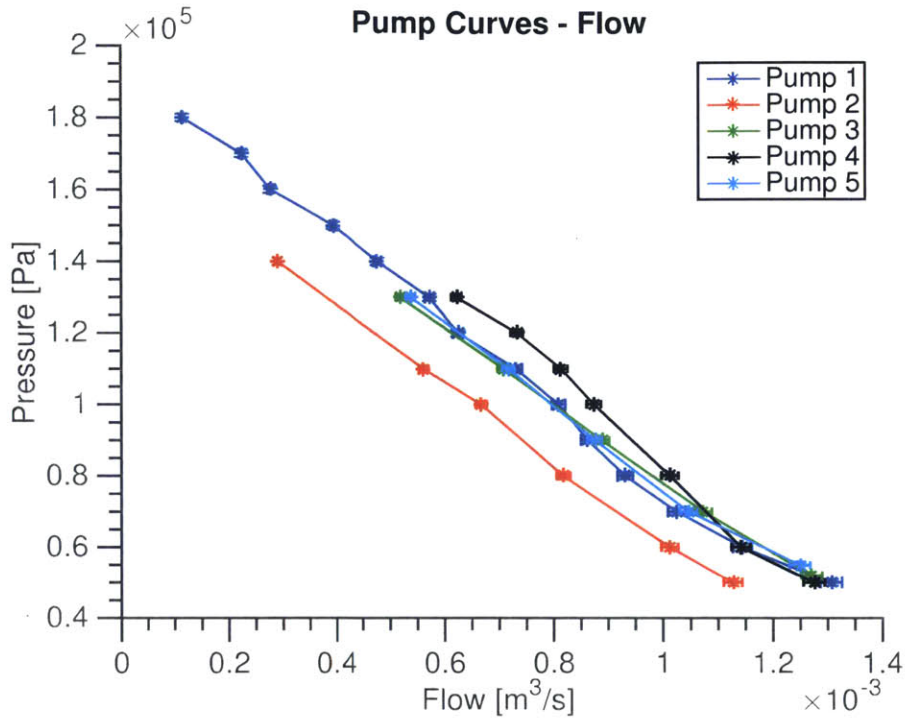


Figure 4-2: Results of pump testing

4.2 Experimental Results

Five pumps were built and tested. The results of these tests showing pressure, power draw, and efficiency vs flow rate can be seen in Fig. 4-2, 4-3, and 4-4. First of all, as can be seen in Fig. 4-2, our performance point of 13 gal/min (here in metric as $0.8\text{m}^3/\text{s}$) and a pressure of 1 bar (also in metric at 100 kPa) was met. However, a great deal of variation between the pumps can be seen. One can also see that our most efficient (represented by the black line in each figure) reaches an efficiency 29% which is short of our goal of 35%. This leads to a power draw of 305 watts at our performance point which is greater than what was expected. This is easily explained by the uncharacteristically low efficiency of our motor, which was 62% efficient. With a more typical brushless DC motor with 90% efficiency, a pump with our impeller and volute could achieve an efficiency of 42%. This would give us a power draw of 190 watts which is lower than the 235 watts expected.

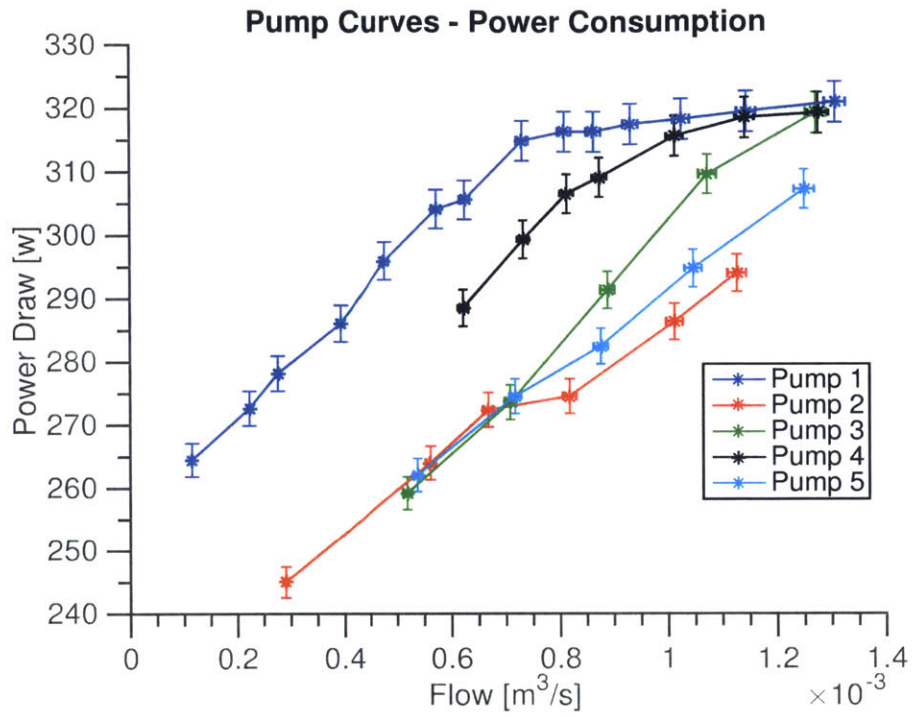


Figure 4-3: Results of pump testing

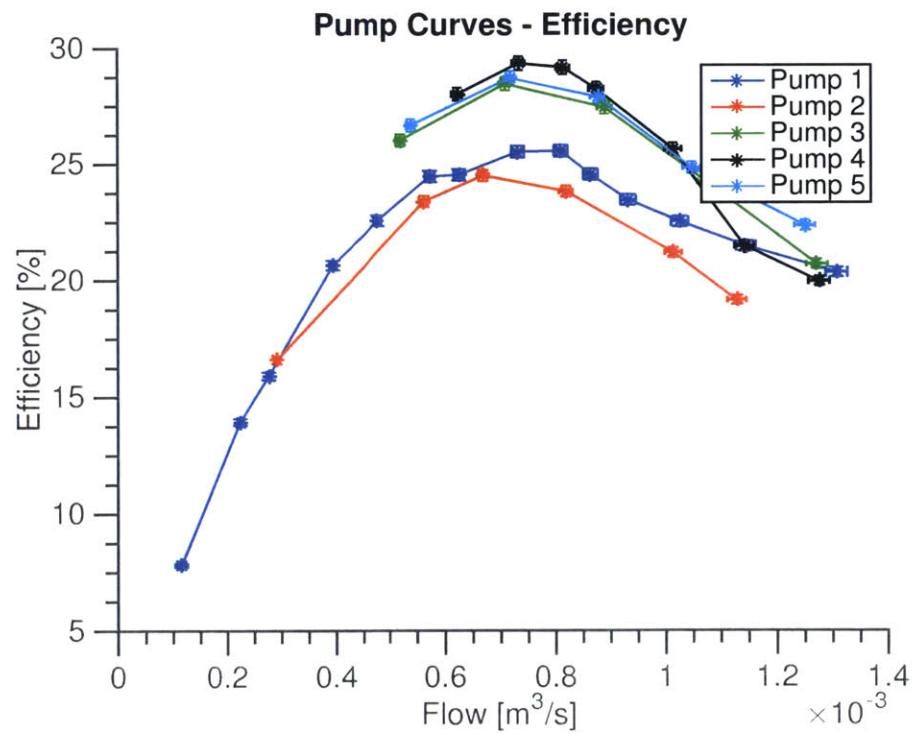


Figure 4-4: Results of pump testing

4.3 Pilot Study

As of February 2015, two pilot studies of the system are taking place in the villages of Jenasai and Sombra, near the town of Chakradharpur, Jharkhand.

4.3.1 System Adjustments

Given that the pump that was designed and built had a much larger power draw than what the rest of the system was designed for, some adjustments had to be made. This includes increasing the battery storage to two 12 volt, 9 amp-hour batteries (as opposed to 7 amp-hours). 300 watts of panels (two 150 watt panels) were still used in order to keep the number of solar panels the farmer had to carry manageable and because the panels represent the bulk of the system cost. Because the power from the panels was not sufficient to power the pump on its own at any time, the batteries needed to be charged while the pump was off in order to assist the panels when the pump was running. In order to accomplish this, a hard timer was programmed into an Arduino Uno and allowed the battery to charge for 25 minutes before the Arduino signals a motor controller to turn on the pump. Once the pump ran out the battery, which the Arduino was powered by, the Arduino would shut down for a few seconds until the solar panels charged the batteries enough to power the Arduino and the timer would start again. This reduction in running time led to a reduction in the amount of water total per day by about half of what we expected. Fortunately, rather than using flood irrigation the farmers we are working with employ an efficient irrigation technique in which they fill a plastic lined hole called a jalcund (Fig 4-7), fill watering cans from the jalcund and spot water the plants. For this reason, we were still providing enough water to allow them to irrigate.



Figure 4-5: Panels, charge controller, motor controller, Arduino Uno, and batteries wired up for use along with some tools for debugging.

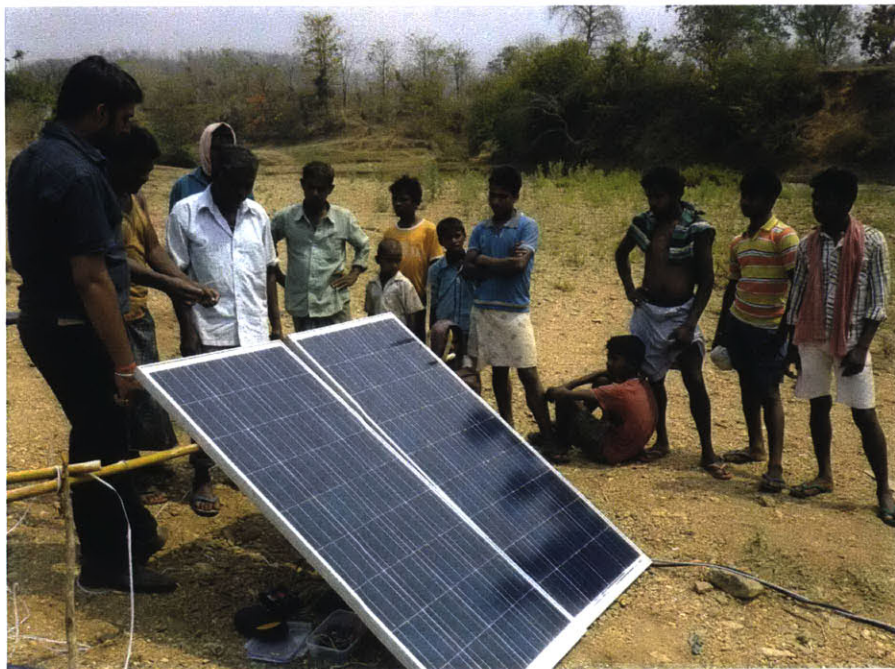


Figure 4-6: Solar panels leaning on a bamboo structure made by the farmers at Sombra.



Figure 4-7: A plastic lined hole called a jalcund that gets filled with water. The water flowing into the jalcund is being lifted by our pump.

Chapter 5

Conclusions and Future Work

As was explained in Section 4.2, although a the pump that was designed did not meet the 35% efficiency goal (instead getting 29% efficiency), it is still at a much higher efficiency point than any other pump of its kind on the market. Also, by replacing the current motor with a more efficient one, an efficiency of 42% can be reached. Further work includes getting a more accurate cost of the system, acquiring said high efficiency motor, designing a more repeatable manufacturing process and improving the electronics design to manage power moving between the pump, panels, and batteries. There are also plans to redesign each of the pump parts with large scale manufacturing in mind.

As of the writing of this thesis, the farmers in Jenasai and Sombra have continued to use our system and are irrigating in the Dry season for the very first time. We plan on continuing to work with these farmers and improve the pump and system to further meet their needs. The project will be continued through the Global Founder's Startup Accelerator at the Martin Trust Center at MIT, with the goal of starting a company so that we can help as many farmers as we can irrigate through the year.

Bibliography

- [1] India solar resource, global horizontal irradiance - march. Technical report, National Renewable Energy Laboratory, 2015.
- [2] H. H. Anderson. Prediction of head, quantity and efficiency in pumps - the area ratio principle. *Performance of Centrifugal Pumps and Compressors.*, 1980.
- [3] Central Ground Water Board. Ground water scenario, premonsoon 2014. Technical report, Ministry of Water Resources, Government of India, 2014.
- [4] Aditi Mukherji et al. Major insights from india's minor irrigation censuses: 1986-87 to 2006-07. *Review of Rural Affairs*, 2013.
- [5] Igor J. Karassik. *Pump Handbook*. McGraw Hill, 2008.
- [6] Kevin Simon. Applications of design for value to distributed solar generation in indian food processing and irrigation. Master's thesis, Massachusetts Institute of Technology, 2015.
- [7] A. J. Stepanoff. *Centrifugal and Axial Flow Pumps*. Krieger Publishing, 1957.